Periyodik Olmayan Oluklu Duvarlara Sahip Paralel Plakalı Dalga Kılavuzunun Analizi

Hacı Bekir Abanuzoğlu

YÜKSEK LİSANS TEZİ

Elektrik-Elektronik Mühendisliği Anabilim Dalı

Mart 2023

Analysis of Parallel Plate Waveguides with Nonperiodically Corrugated Walls

Hacı Bekir ABANUZOĞLU

MASTER OF SCIENCE THESIS

Department of Electrical and Electronics Engineering

March 2023

Analysis of Parallel Plate Waveguides with Nonperiodically Corrugated Walls

Hacı Bekir ABANUZOĞLU

A thesis submitted to Eskişehir Osmangazi University

Graduate School of Natural and Applied Sciences in partial

fulfillment of the requirements for the degree of Master of Science

in Discipline of Electromagnetic Fields and Microwave Techniques of the Department of Electrical and Electronics Engineering

by
Hacı Bekir ABANUZOĞLU

Supervisor: Prof. Dr. Gökhan Çınar

March 2023

APPROVAL OF THE THESIS

The thesis titled “Analysis of Parallel Plate Waveguides with Nonperiodically Corrugated Walls” and submitted by Hacı Bekir ABANUZOĞLU has been accepted as satisfactory in partial fulfillment of the requirements for the degree of Master of Science in Department of Electrical and Electronics Engineering.

Supervisor: Prof. Dr. Gökhan ÇINAR
Co-Supervisor: -

Examining Committee Members:

Member: Prof. Dr. Gökhan ÇINAR

Member: Assoc. Prof. Dr. Hayrettin ODABASI

Member: Prof. Dr. Nihan KOSKU PERKGÖZ

Graduation of Hacı Bekir ABANUZOĞLU was approved by the Graduate School Board Decision on .... with the decision number of ....

Prof. Dr. Hürriyet ERŞAHAN
Director of the Institute

ETHICAL STATEMENT

I hereby declare that this thesis study entitled "Analysis of Parallel Plate Waveguides with Nonperiodically Corrugated Walls" has been prepared in accordance with the thesis writing rules of Eskişehir Osmangazi University Graduate School of Natural and Applied Sciences under academic consultancy of my supervisor Prof. Dr. Gökhan ÇINAR. I hereby declare that the work presented in this thesis is original. I also declare that, I have respected scientific ethical principle and rules in all stages of my thesis study, all information and data presented in this thesis have been obtained within the scope of scientific and academic ethical principles and rules, all materials used in this thesis which are not original to this work have been fully cited and referenced, and all knowledge, documents and results have been presented in accordance with scientific ethical principles and rules.

22/03/2023

Hacı Bekir ABANUZOĞLU

ÖZET

Elektromanyetik dalgalar uzayda her yöne yayıldıklarında yayılım şiddeti mesafenin karesiyle ters orantılı olarak azalır, bu radyasyon şiddetinin azalması sorununun üstesinden gelmek için elektromanyetik dalgaların, dalga kılavuzları yardımıyla sadece bir yönde yayılım yapması sağlanabilir. Ancak dalga kılavuzu kullanımı elektromanyetik yayılımla ilgili problemleri tamamen çözemez çünkü dalga kılavuzlarının güç aktarım karakteristikleri geometrilerine bağlıdır. Bu yüzdendir ki; bir tasarım yaparken deneme yanılma metotlarının ötesine gitmek için, bu geometrileri analiz edebilecek matematiksek araçlar geliştirmek gerekmektedir. Günümüzde çeşitli amaçlar için kullanılabilecek çok amaçlı elektromanyetik simülasyon yazılımları mevcuttur (ör., CST Studio, HFSS, AWR, Analyst, NEC, vb.). Ancak bu simülasyon yazılımlarının varlığı geliştirilen analitik modelleri işlevsiz kılmamaktadır çünkü analitik yöntemler hesap yönünden nümerik simülasyonlardan çok daha az bir işlem gücü gerektirmektedir.

Bu çalışmada periyodik olmayan oluklu duvarlara sahip paralel plaka dalga kılavuzları incelendi ve bunu yaparken önce dalga kılavuzlarının saçılma matrislerinin hesaplanmasını sağlayan matematiksel formüller türetildi. Farklı parametrelere sahip yapıların saçılma parametreleri hesaplandı ve birbirleriyle ve aynı zamanda periyodu oluklu duvarlara sahip dalga kılavuzu karşılıklarıyla kıyaslanarak aralarındaki benzerlikler ve sapmalar incelendi.

Periyodik olmayan oluklu duvarlara sahip paralel plakalı dalga kılavuzlarını incelemek için, mod eşleştirme tekniğinden faydalanılarak matematiksel bir yöntem geliştirildi. Mod eşleştirme tekniği süreksizliklerde elektromanyetik dalgaların davranışlarını belirleyebileceğimiz isabetli bir metottur. Mod eşleştirme tekniği sınır koşullarını uygularken, sinüzoidal fonksiyonların ortogonallik özelliğinden faydalanarak süreksizliğin her iki tarafındaki alanların genlikleri arasında bir ilişki kurar. Genlikler arasındaki ilişkiyi gösteren matematiksel ifadeler kullanılarak da genelleştirilmiş saçılım matrisleri hesaplanır. Eğer süreksizlikler için saçılma matrisleri mod eşleme yöntemiyle elde

edilirse, süreksizliklerin birbirini takip ettiği bir yapıda her bir süreksizliğe karşılık gelen saçılım matrislerini birbirleriyle kaskadlayarak bütün bir yapının saçılma matrisleri elde edilebilir.

Elde edilen model periyodik olmayan oluklu duvarlara sahip paralel plaka dalga kılavuzlarının davranışlarını incelemek için kullanılacaktır, ancak bu model paralel plaka yapısına sahip örneğin bir filtre gibi herhangi elektromanyetik bir cihazın incelenmesi veya tasarımı için kullanılabilir. Üstelik elimizde parametreleri belli olan süreksizliklere sahip bir paralel plaka dalga kılavuzunun saçılma matrisini veren bir model olduğu için mu modeli çeşitli optimizasyon ve makine öğrenmesi algoritmalarıyla birleştirerek arzulanan karakteristiklere sahip yapılar elde etmek mümkün olabilecektir.

Son olarak mod eşleme yöntemiyle simülasyonlara oranla azaltılmış işlem yükünü daha da azaltmak adına oluklu duvarların empedans yüzeyleriyle değiştirilerek saçılma matrislerinin hesaplandı. Empedans yüzeyleriyle değiştirilerek elde edilen sonuçlarla aynı yapılar için mod eşleme yönteminin verdiği sonuçlar karşılaştırılarak ne kadar geniş bir yelpazede çalışabildikleri incelendi.

Bu çalışmada belirtilen matematiksel model ve yöntemlerin gerçekleştirilmesi NumPy, Matplotlib, ve Pandas kütüphaneleri yüklü olan bir Python ortamında yapılmıştır. Mod eşleştirme tekniğiyle elde edilen analitik sonuçlarla CST studio kullanılarak elde edilen simülasyonlar karşılaştırılarak geliştirilen formülasyonların doğruluğu test edilmiştir.

Anahtar kelimeler: Paralel Plakalı Dalga Kılavuzları, TE Dalga Yayılımı, Oluklu Duvarlı Dalga Kılavuzları, Mod Eşleştirme Tekniği, Genelleştirilmiş Saçılım Matrisleri, Empedans Yüzeyleri

SUMMARY

In this study, parallel plate waveguides with non-periodically corrugated walls are analyzed using mode-matching techniques. Mode-matching technique is a very accurate method for determining behaviors of electromagnetic waves at discontinuities. It uses the advantage of orthogonality of sinusoidal functions apparent in expressions of field components for each mode while applying boundary conditions at discontinuity. Once relations between backward and forward travelling waves are derived from boundary conditions, the Scattering Matrix can be obtained. After obtaining the scattering matrix for a discontinuity one can cascade those scattering matrices together to obtain a Generalized Scattering Matrix for a structure that consists of multiple discontinuities.

Implementation of this study is done in a Python environment with NumPy, Matplotlib and Pandas libraries installed. Results that are obtained from the derived analytical method are compared with results from CST Studio Suite 2022 for verification of the implemented algorithm.

Keywords: Parallel Plate Waveguides, TE Wave Propagation, Parallel Plate Waveguide with Corrugated Walls, Mode Matching Technique, Impedance Surfaces

ACKNOWLEDGEMENT

I’m deeply indebted to my advisor Prof. Dr. Gökhan ÇINAR for his immeasurable, both academic and scientific support and guidance through my master’s degree.

My sincere thanks also go to Assoc. Prof. Dr. Hayrettin ODABAŞI and Dr. Mohammed A.I. MATAR for sharing their valuable insights about electromagnetic theory.

I would also like to express my gratitude to all my lecturers from whom I learned a lot during my study in Eskişehir Osmangazi University.

Finally, I cannot conclude without thanking my family for their support in every. stage of my life. I feel too fortunate to have had them as my family.

LIST OF CONTENTS

Page

LIST OF FIGURES

LIST OF FIGURES (continued)

LIST OF ABBREVIATIONS AND SYMBOLS

Symbols	**Descriptions**
ϵ	Permitivity of free space
μ	Permeability of free space
ω	Angular Frequency
f_c	Cutoff Frequency
β	Propagation constant
E	Electric Field
H	Magnetic Field

Abbreviations	**Descriptions**
CST Studio	Electromagnetic Simulation Software
MMT	Mode Matching Technique

1. INTRODUCTION AND PURPOSE

When an electromagnetic wave propagates in space it propagates in all directions, so intensity of the radiation decreases due to inverse square law. To overcome this waste of energy, electromagnetic waves can be confined inside certain structures via the help of waveguides.

Use of waveguides does not suddenly solve all the problems because power transfer characteristics of a waveguide depends on its geometry as well. In order to go beyond trial and error while designing and analyzing waveguides, one must first develop necessary mathematical models for analyzing interested geometries or use existing methods and simulation softwares. Nowadays there is an abundance of simulation softwares (i.e., CST Studio, HFSS, AWR Analyst, NEC, etc.) for electromagnetics systems so one can use an available simulation software for design and analysis. The existence of this variety of softwares doesn't negate the benefits of developing analytical models because numerical simulations can demand much more computing power when compared to analytical methods.

Even if we completed every design step before production of let's say a filter, there is no such thing as a flawless production process every production method will introduce some random irregularities to the material, and these irregularities will effect its electromagnetic characteristics so designer may need to account for these effects. Goal of this study is to develop a model that predict characteristic of aperiodic corrugations. One can also think these aperiodic corrugations as random roughness of a surface and use it to model irregularities of an electromagnetic device.

In this study, in order to analyze parallel plate waveguides with non-periodically corrugated walls, an analytical model is developed. When deriving this mathematical model, mode-matching technique (MMT) is used to generate field relations for backward and forward traveling waves for regions on both sides of a discontinuity and using these field relations Scattering Matrices are obtained via algebraic manipulations. In MMT, in order to get exact field expressions, one must consider an infinite number of modes in calculations which in practice is not feasible because of finite computer memories. Despite these limitations, accurate results can be achieved via choosing an adequate number of modes to include in calculation. In this study, the effect of mode truncation on accuracy was also inspected. After having mathematical expressions for a discontinuity, one can cascade these discontinuities to achieve results for a geometry with multiple discontinuities.

After deriving necessary mathematical formulation, the model is implemented in the Python programming language. Verification of the implementation is done by comparing CST Studio and Mode-Matching implementation results of various relatively small geometries (i.e., 5, 6, 7 discontinuities cascaded). After being convinced that implementation is giving accurate results, the only job left is to analyze the geometry using the implemented python code. The aperiodicity of the structures is achieved by setting groove parameters in a manner that represents parallel waveguide with non-periodically corrugated walls.

2. LITERATURE REVIEW

Various analytical and numerical methods can be used when analyzing corrugated structures, Hänninen and Nikoskinen (2008) developed a method of moment formulation to analyze scattering of corrugated surfaces by using impedance boundary conditions. The numerical analysis of the impedance surface is done using closed-form formulae and accurate numerical integration. The studied formulation greatly decreases the computational resources required to study corrugated structures. Sipus and Kildal (2002) derived Green's functions in the spectral domain for corrugated surfaces by using asymptotic corrugation boundary conditions with the assumption that periodicity of corrugations was less than wavelength.

Mode matching technique is a very useful analytic method in the analysis of waveguide discontinuities due to its simplicity, accuracy, and high performance over numerical methods. Hence, it's beneficial to employ mode matching techniques whenever it's feasible. Wexler (1967) presented a general method for analyzing waveguide junctions, deriving solutions for scattered modes by summing normal modes of propagations. In the modal analysis method, the amplitudes of normal modes are chosen so as to satisfy boundary conditions at the discontinuity. Because the modal approach is direct and conforms closely to physical reality, it should have the widest application. (Wexler, 1967). Ghasemifard et al. (2017) used mode matching technique for analyzing two dimensional doubled corrugated metasurfaces and obtained an analytical method that is very fast and results are compliant with the numerical full wave simulations. The formulation is general as it can be employed to obtain the dispersion diagram of conventional, mirrored, and glide-symmetric corrugated waveguides. Coccioli et al. (1996) presented a hybrid mode matching-integral equation method for the analysis and design of corrugated horns which achieves accurate prediction of radiation and input impedance properties.

Uusitupa (2006) investigated error when when using approximate corrugation models in scattering analysis.

3. MATERIALS AND METHOD

3.1. Helmholtz Equations

In source-free, linear, isotropic, homogeneous region, Maxwell's equations can be written in phasor form as follows,

$$\boldsymbol{\nabla} \times \boldsymbol{E} = -\mathrm{j}\omega\mu H \tag{3.1a}$$

$$\boldsymbol{\nabla} \times \boldsymbol{H} = \mathrm{j}\omega\epsilon\boldsymbol{E} \tag{3.1b}$$

Inserting expression for H obtained from (3.1a) into (3.1b) yields,

$$\boldsymbol{\nabla} \times \boldsymbol{\nabla} \times \boldsymbol{E} = \omega^2\mu\epsilon\boldsymbol{E} \tag{3.2}$$

Curl operations in (3.2) can be eliminated using $\nabla \times \nabla \times \overline{\mathrm{A}} = \nabla(\nabla \cdot \overline{\mathrm{A}}) - \nabla^2\overline{\mathrm{A}}$ vector identity.

$$\boldsymbol{\nabla}^{\boldsymbol{2}}\boldsymbol{E} + \omega^2\mu\epsilon\boldsymbol{E} = 0 \tag{3.3}$$

Same wave equation can be derived for magnetic field via applying same procedure:

$$\boldsymbol{\nabla}^{\boldsymbol{2}}\boldsymbol{H} + \omega^2\mu\epsilon\boldsymbol{H} = 0 \tag{3.4}$$

3.2. TE Modes on Parallel Plate Waveguides

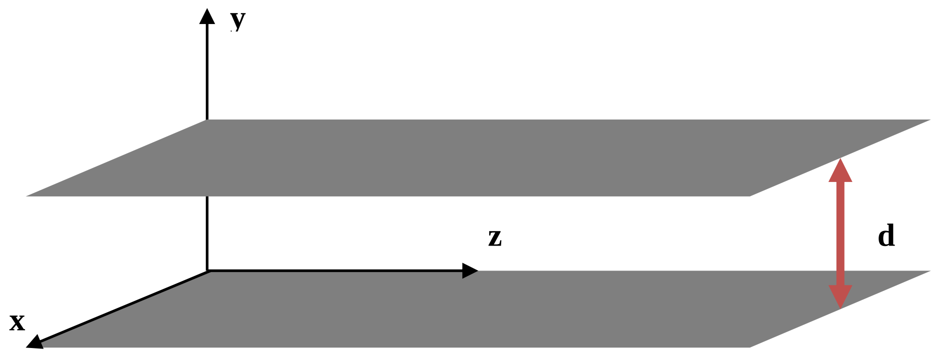

Figure 3. 1. Structure of parallel plate waveguide

We assume wave propagates along z axis with e^{jwt} time dependency in source-free, linear, isotropic, homogeneous region. Electric and magnetic fields can be written as

$$\boldsymbol{E}(x,y,z) = \left[\hat{x}E_x^0(x,y) + \hat{y}E_y^0(x,y) + \hat{z}E_z^0(x,y)\right]\mathrm{e}^{-\mathrm{j}\beta z} \tag{3.5a}$$

$$\boldsymbol{E}(x,y,z) = \left[\hat{x}H_x^0(x,y) + \hat{y}H_y^0(x,y) + \hat{z}H_z^0(x,y)\right]\mathrm{e}^{-\mathrm{j}\beta z} \tag{3.5b}$$

Where β is the propagation constant, the wave is propagating $+z$ direction, expression for $-z$ direction can be obtained via changing $\mathrm{e}^{-\mathrm{j}\beta z}$ to $\mathrm{e}^{\mathrm{j}\beta z}$.

By inserting field expressions from equations (3.5a) and (3.5b) into (3.1a) and (3.1b) (note that because of $\mathrm{e}^{-\mathrm{j}\beta z}$ z dependence $\frac{\partial}{\partial z} = -\mathrm{j}\beta$)

$$\begin{bmatrix} \hat{x} & \hat{y} & \hat{z} \\ \dfrac{\partial}{\partial x} & \dfrac{\partial}{\partial y} & \dfrac{\partial}{\partial z} \\ E_x & E_y & E_z \end{bmatrix} = -\mathrm{j}\omega\mu(\hat{x}H_x + \hat{y}H_y + \hat{z}H_z) \tag{3.6a}$$

$$\begin{bmatrix} \hat{x} & \hat{y} & \hat{z} \\ \dfrac{\partial}{\partial x} & \dfrac{\partial}{\partial y} & \dfrac{\partial}{\partial z} \\ E_x & E_y & E_z \end{bmatrix} = \mathrm{j}\omega\epsilon\left(\hat{x}E_x + \hat{y}E_y + \hat{z}E_z\right) \tag{3.6b}$$

From equations (3.6a) and (3.6b), equations below can be derived for each component of field vectors,

$$\frac{\partial E_z}{\partial y} + \mathrm{j}\beta E_y = -\mathrm{j}\omega\mu H_x \tag{3.7a}$$

$$-\mathrm{j}\beta E_x - \frac{\partial E_z}{\partial x} = -\mathrm{j}\omega\mu H_y \tag{3.7b}$$

$$\frac{\partial E_y}{\partial x} - \frac{\partial E_x}{\partial y} = -\mathrm{j}\omega\mu H_z \tag{3.7c}$$

$$\frac{\partial H_z}{\partial y} + \mathrm{j}\beta H_y = \mathrm{j}\omega\epsilon E_x \tag{3.8a}$$

$$-\mathrm{j}\beta H_x - \frac{\partial H_z}{\partial x} = -\mathrm{j}\omega\epsilon E_y \tag{3.8b}$$

$$\frac{\partial H_y}{\partial x} - \frac{\partial H_x}{\partial y} = -\mathrm{j}\omega\epsilon E_z \tag{3.8c}$$

If we solve above six equations in terms of $E_z\, and\, H_z$ for E_x, E_y, H_x, H_y components, following expressions can be derived,

$$H_x = \frac{\mathrm{j}}{k_c^2}\left(\omega\epsilon\frac{\partial E_z}{\partial y} - \beta\frac{\partial H_z}{\partial x}\right) \tag{3.9a}$$

$$H_y = -\frac{\mathrm{j}}{k_c^2}\left(\omega\epsilon\frac{\partial E_z}{\partial x} + \beta\frac{\partial H_z}{\partial y}\right) \tag{3.9b}$$

$$E_x = -\frac{\mathrm{j}}{k_c^2}\left(\beta\frac{\partial E_z}{\partial x} + \omega\mu\frac{\partial H_z}{\partial y}\right) \tag{3.9c}$$

$$E_y = \frac{\mathrm{j}}{k_c^2}\left(-\beta\frac{\partial E_z}{\partial y} + \omega\mu\frac{\partial H_z}{\partial x}\right) \tag{3.9d}$$

k_c in above equation is defined as cutoff wave number

$$k_c^2 = k^2 - \beta^2 \tag{3.10}$$

$$k = \omega\sqrt{\mu\epsilon} = \frac{2\pi}{\lambda} \tag{3.11}$$

This study focuses on propagation of TE modes hence $E_z = 0$ and $H_z \neq 0$ therefore equations (3.9) reduce to

$$H_x = -\frac{\mathrm{j}\beta}{k_c^2}\frac{\partial H_z}{\partial x} \tag{3.12a}$$

$$H_y = -\frac{\mathrm{j}\beta}{k_c^2}\frac{\partial H_z}{\partial y} \tag{3.12b}$$

$$E_x = -\frac{\mathrm{j}\omega\mu}{k_c^2}\frac{\partial H_z}{\partial y} \tag{3.12c}$$

$$E_y = \frac{\mathrm{j}\omega\mu}{k_c^2}\frac{\partial H_z}{\partial x} \tag{3.12d}$$

TE mode wave impedance:

$$Z_{TE} = \frac{E_x}{H_y} = -\frac{E_y}{H_x} = \frac{\omega\mu}{\beta} = \frac{k\eta}{\beta} \tag{3.13}$$

To apply (3.12), H_z must be found using Helmholtz wave equation,

$$\left(\frac{\partial^2}{\partial x^2} + \frac{\partial^2}{\partial y^2} + \frac{\partial^2}{\partial z^2} + k^2\right) H_z = 0 \tag{3.14}$$

Since $H_z(x, y, z) = H_z(x, y)e^{-j\beta z}$ (3.14) can be reduced as follows,

$$\left(\frac{\partial^2}{\partial x^2} + \frac{\partial^2}{\partial y^2} + k_c^2\right) H_z(x, y) = 0 \tag{3.15}$$

Because of structure of parallel plate waveguide and characteristics of TE modes $\frac{\partial}{\partial x} = 0$ so (3.15) reduces further to:

$$\left(\frac{\partial^2}{\partial y^2} + k_c^2\right) H_z(x, y) = 0 \tag{3.16}$$

General solution of (3.16) is

$$H_z(x, y) = Asin(k_c y) + Bcos(k_c y) \tag{3.17}$$

In order to find A and B in (3.17) boundary conditions must be utilized. Boundary conditions for said structure is,

$$E_x = 0 \; at \; y = 0 \; and \; y = d \tag{3.18}$$

Expression for E_x can be found by using (3.17) and (3.12c)

$$E_x = -\frac{\mathrm{j}\omega\mu}{k_c}\left(Acos(k_c y) - Bsin(k_c y)\right)\mathrm{e}^{-\mathrm{j}\beta z} \tag{3.19}$$

Applying boundary condition from (3.18) to (3.19) results $A = 0$ at $y = 0$ and at $y = d$,

$$k_c = \frac{n\pi}{d}, \qquad n = 1, 2, 3 \ldots \tag{3.20}$$

Final solution for H_z becomes,

$$H_z = B_n \cos\left(\frac{n\pi y}{d}\right) \mathrm{e}^{-\mathrm{j}\beta z} \tag{3.21}$$

$$E_x = \frac{\mathrm{j}\omega\mu}{k_c} B_n \sin\left(\frac{n\pi y}{d}\right) \mathrm{e}^{-\mathrm{j}\beta z} \tag{3.22a}$$

$$H_y = \frac{\mathrm{j}\beta}{k_c} B_n \sin\left(\frac{n\pi y}{d}\right) \mathrm{e}^{-\mathrm{j}\beta z} \tag{3.22b}$$

$$E_y = H_x = 0 \tag{3.22c}$$

Propagation constant and cutoff frequency for a given TE_n *mode is*

$$\beta = \sqrt{k^2 - \left(\frac{n\pi}{d}\right)^2} \tag{3.23}$$

$$f_c = \frac{n}{2d\sqrt{\mu\epsilon}} \tag{3.24}$$

3.3. Mode Matching Technique for H-Plane Discontinuity

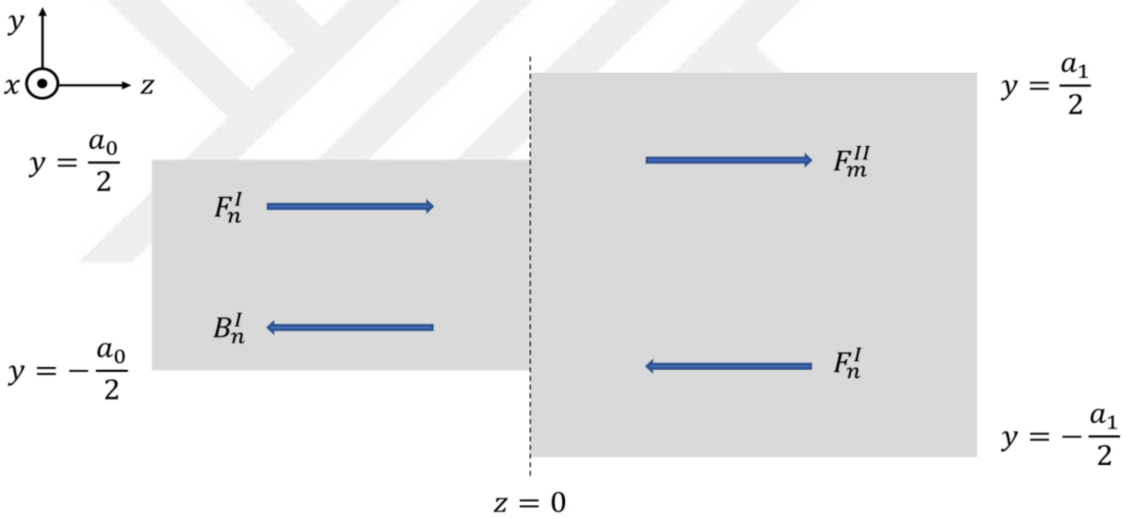

Figure 3. 2. Structure of discontinuity

For given structure (Figure 3.2.) propagation constants for propagating and evanescent modes is

$$\beta_m^x = \begin{cases} \sqrt{\omega^2\mu\epsilon - \left(\frac{m\pi}{a_x}\right)^2}, & \textit{propagating mode} \\ -\mathrm{j}\sqrt{\left(\frac{m\pi}{a_x}\right)^2 - \omega^2\mu\epsilon}, & \textit{evanescent mode} \end{cases} \tag{3.25}$$

Using (3.22a) and (3.22b) equations and wave admittance, field expressions for the first and second region can be written as:

$$E_x^I = \sum_{m=1}^{\infty} G_m^I \sin\left(\frac{m\pi\left(y+\frac{a_0}{2}\right)}{a_0}\right)\left(F_m^I \mathrm{e}^{-\mathrm{j}\beta_m^I z} + B_m^I \mathrm{e}^{\mathrm{j}\beta_m^I z}\right) \tag{3.26a}$$

$$\mathrm{H_y^I} = \sum_{m=1}^{\infty} G_m^I Y_m^I \sin\left(\frac{m\pi\left(y+\frac{a_0}{2}\right)}{a_0}\right)\left(F_m^I \mathrm{e}^{-\mathrm{j}\beta_m^I z} - B_m^I \mathrm{e}^{\mathrm{j}\beta_m^I z}\right) \tag{3.26b}$$

$$E_x^{II} = \sum_{n=1}^{\infty} G_n^{II} \sin\left(\frac{n\pi\left(y+\frac{a_1}{2}\right)}{a_1}\right)\left(F_n^{II} \mathrm{e}^{-\mathrm{j}\beta_n^{II} z} + B_n^{II} \mathrm{e}^{\mathrm{j}\beta_n^{In} z}\right) \tag{3.26c}$$

$$\mathrm{H_y^{II}} = \sum_{n=1}^{\infty} G_n^{II} Y_n^{II} \sin\left(\frac{n\pi\left(y+\frac{a_1}{2}\right)}{a_1}\right)\left(F_n^{II} \mathrm{e}^{-\mathrm{j}\beta_n^{II} z} - B_n^{II} \mathrm{e}^{\mathrm{j}\beta_n^{II} z}\right) \tag{3.26d}$$

Where Y_m^k is wave admittance of mth mode in kth region,

$$Y_m^k = \frac{\beta_m^k}{\omega\mu} \tag{3.27}$$

For simplicity G_m^I (Normalization factor) is used to normalize average power and calculated by limiting maximum power each mod can carry to $1W$ for a maximum wave amplitude $F_m^I = 1\sqrt{\mathrm{W}}\ and\ B_m^I = 0$.

$$P_m^I = \frac{1}{2} Re\{\int_{-\frac{a}{2}}^{\frac{a}{2}} (\boldsymbol{E}_m^I \times \boldsymbol{H}_m^{I*}) dy = 1W \tag{3.28}$$

If we solve (3.28) for G_m^k (mth mode in kth region)

$$G_m^k = 2\sqrt{\frac{\omega\mu}{a_k \beta_m^k}} \tag{3.29}$$

Boundary condition for matching field components at discontinuity ($z = 0$) are as follows,

$$\begin{cases} E_x^{II} = 0, & |y| > \frac{a_0}{2} \\ E_x^{II} = E_y^I, & |y| < \frac{a_0}{2} \end{cases} \tag{3.30a}$$

$$H_y^{II} = H_y^I, \qquad |y| < \frac{a_0}{2} \tag{3.30b}$$

Matching field components (3.26) using (3.30a) and (3.30b) at $z = 0$

$$\sum_{m=1}^{\infty} G_m^I \sin\left(\frac{m\pi\left(y+\frac{a_0}{2}\right)}{a_0}\right)(F_m^I + B_m^I) = \sum_{n=1}^{\infty} G_n^{II} \sin\left(\frac{n\pi\left(y+\frac{a_1}{2}\right)}{a_1}\right)(F_n^{II} + B_n^{II}) \tag{3.31}$$

$$\sum_{m=1}^{\infty} G_m^I Y_m^I \sin\left(\frac{m\pi\left(y+\frac{a_0}{2}\right)}{a_0}\right)(F_m^I - B_m^I) = \sum_{n=1}^{\infty} G_n^{II} Y_n^{II} \sin\left(\frac{n\pi\left(y+\frac{a_1}{2}\right)}{a_1}\right)(F_n^{II} - B_n^{II}) \tag{3.32}$$

In order to isolate the amplitudes of forward and backward travelling waves orthogonality of sinusoids used. According to boundary conditions tangential electrical field on the surface of the metal step must be equal to zero, as opposed to magnetic field so when choosing interval for integration, larger interval always used for E field expressions, and smaller one for H field therefore there is a mathematical difference between widening and narrowing discontinuities for example for a widening discontinuity bounds of integral for electric field will be width of the second region because it is larger interval of two. In case of narrowing discontinuities interval of integration will be the width of first region because it is smaller one of two.

In order to isolate amplitudes in second region in E field expression (3.31), we multiply it with $\sin\left(\frac{n'\pi\left(y+\frac{a_1}{2}\right)}{a_1}\right)$ then integrate over the larger interval, integral referring to second region only become nonzero when $n' = n$ so we get expression below,

$$F_n^{II} + B_n^{II} = \sum_{m=1}^{\infty} \frac{2G_m^I}{a_1 G_n^{II}} \int_{-\frac{a_1}{2}}^{\frac{a_1}{2}} \sin\left(\frac{m\pi\left(y+\frac{a_0}{2}\right)}{a_0}\right) \sin\left(\frac{n\pi\left(y+\frac{a_1}{2}\right)}{a_1}\right) dy (F_m^I + B_m^I) \qquad (3.33)$$

$$LE_{nm} = \frac{2G_m^I}{a_1 G_m^I} \int_{-\frac{a_1}{2}}^{\frac{a_1}{2}} \sin\left(\frac{m\pi\left(y+\frac{a_0}{2}\right)}{a_0}\right) \sin\left(\frac{n\pi\left(y+\frac{a_1}{2}\right)}{a_1}\right) dy \qquad (3.34)$$

$$F^{II} + B^{II} = L_E(F^I + B^I) \qquad (3.35)$$

In order to isolate amplitudes of H field expression in first region in (3.32), we multiply it with $\sin\left(\frac{m'\pi\left(y+\frac{a_0}{2}\right)}{a_0}\right)$ then integrate over smaller interval, integral referring to smaller interval becomes nonzero only when $m' = m$ so we get following equations,

$$(F_m^I - B_m^I) = \sum_{n=1}^{\infty} \frac{2G_n^{II} Y_n^{II}}{a_0 G_m^I Y_m^I} \int_{\frac{-a_0}{2}}^{\frac{a_0}{2}} \sin\left(\frac{n\pi\left(y+\frac{a_1}{2}\right)}{a_1}\right) \sin\left(\frac{m'\pi\left(y+\frac{a_0}{2}\right)}{a_0}\right) dy\, (F_n^{II} - B_n^{II}) \qquad (3.36)$$

$$LH_{mn} = \frac{2G_n^{II}Y_n^{II}}{a_0 G_m^I Y_m^I}\int_{\frac{-a_0}{2}}^{\frac{a_0}{2}} \sin\left(\frac{n\pi\left(y+\frac{a_1}{2}\right)}{a_1}\right)\sin\left(\frac{m'\pi\left(y+\frac{a_0}{2}\right)}{a_0}\right)dy \tag{3.37}$$

$$F^I - B^I = L_E(F^{II} - B^{II}) \tag{3.38}$$

Generalized scattering matrix defines relations between amplitudes of forward and backward travelling waves so in our structure above relation between amplitudes is given as

$$\begin{bmatrix} B^I \\ F^{II} \end{bmatrix} = \begin{bmatrix} S_{11} & S_{12} \\ S_{21} & S_{22} \end{bmatrix}\begin{bmatrix} F^I \\ B^{II} \end{bmatrix} \tag{3.39}$$

Using (3.35), (3.38) and (3.39) elements of scattering matrix can be found as

$$S_{11} = (I + L_H L_E)^{-1}(I - L_H L_E) \tag{3.40a}$$

$$S_{12} = 2(I + L_H L_E)^{-1} L_H \tag{3.40b}$$

$$S_{21} = L_E(I + S_{11}) \tag{3.40c}$$

$$S_{22} = L_E S_{12} - I \tag{3.40d}$$

Where I is identity matrix.

3.4. Scattering Matrix for A Homogeneous Waveguide

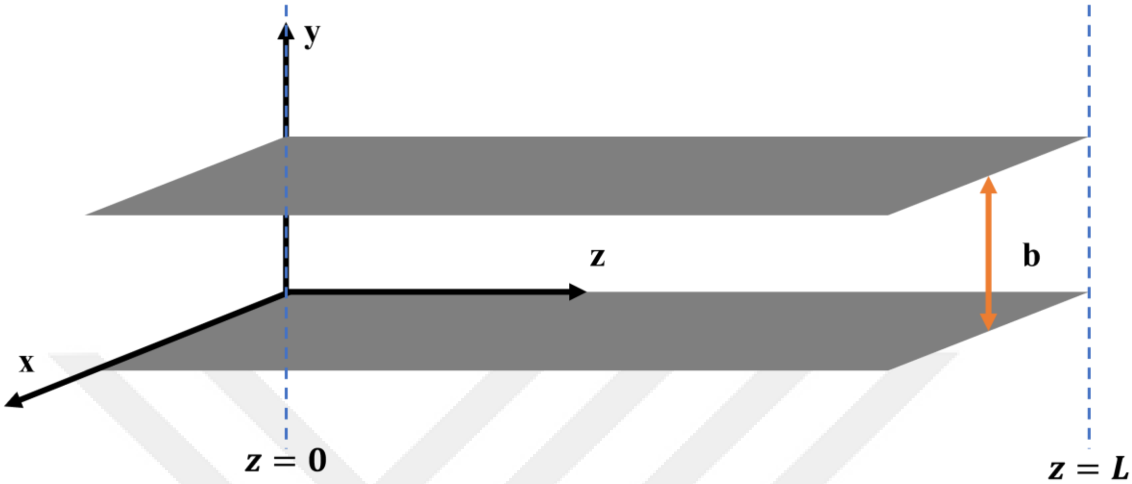

Figure 3. 3. A homogeneous waveguide

To obtain Scattering matrix for a homogeneous waveguide diagonal D matrix, a matrix that contains phase and attenuation information for corresponding mode, can be used. D matrix can be constructed using exponential terms in equations (3.26)

$$D = Diag(\mathrm{e}^{-\mathrm{j}\beta_m L}) \tag{3.41}$$

$$S = \begin{bmatrix} 0 & D \\ D & 0 \end{bmatrix} \tag{3.42}$$

3.5. Cascading Scattering Matrices

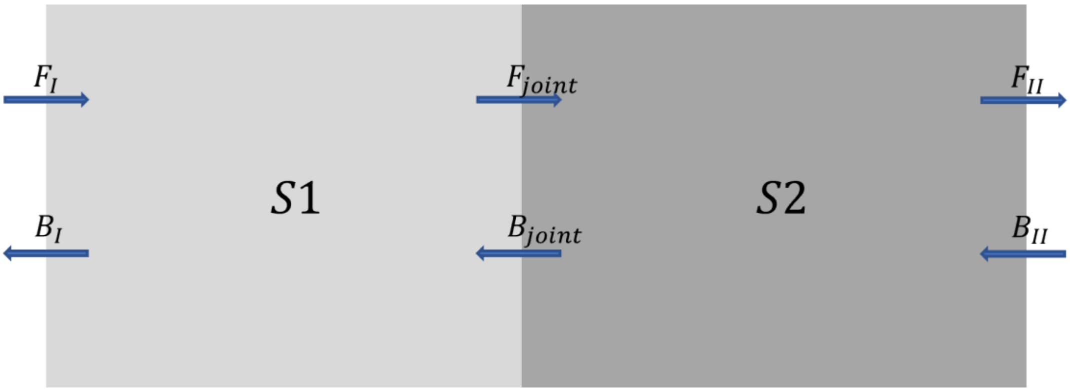

Figure 3. 4. Cascade of scattering matrices (where F_I, B_I and F_{II}, B_{II} are wave amplitudes at port 1 and port 2 respectively, as for F_{joint}, B_{join} are amplitudes at joint)

Given figure above (Figure 3.4) $S1, S2$ (Scattering matrices of first and second region) and S_T (Total scattering matrix) are defined as fallows,

$$\begin{bmatrix} B_I \\ F_{joint} \end{bmatrix} = \begin{bmatrix} S1_{11} & S1_{12} \\ S1_{21} & S1_{22} \end{bmatrix} \begin{bmatrix} F_I \\ B_{joint} \end{bmatrix} \tag{3.43}$$

$$\begin{bmatrix} B_{joint} \\ F_{II} \end{bmatrix} = \begin{bmatrix} S2_{11} & S2_{12} \\ S2_{21} & S2_{22} \end{bmatrix} \begin{bmatrix} F_{joint} \\ B_{II} \end{bmatrix} \tag{3.44}$$

$$\begin{bmatrix} B_I \\ F_{II} \end{bmatrix} = \begin{bmatrix} S_{T11} & S_{T12} \\ S_{T21} & S_{T22} \end{bmatrix} \begin{bmatrix} F_I \\ B_{II} \end{bmatrix} \tag{3.45}$$

Equations (3.43) and (3.44) can be expanded as

$$B_I = S1_{11}F_1 + S1_{12}B_{joint} \tag{3.46a}$$

$$F_{joint} = S1_{21}F_I + S1_{22}B_{joint} \tag{3.46b}$$

$$B_{joint} = S2_{11}F_{joint} + S2_{12}B_{II} \tag{3.47a}$$

$$F_{II} = S2_{21}F_{joint} + S2_{22}B_{II} \tag{3.47b}$$

Where all the terms like Sk_{mn} are submatrices of scattering matrix that contains information about corresponding modes.

In order to find elements of total scattering matrix one first needs to derive expressions for F_{joint} and B_{joint} in terms of F_I and B_{II} because total scattering matrix takes the F_I and B_{II} as inputs.

Using equations (3.46b) and (3.47a), B_{joint} and F_{joint} can be expressed in terms of F_I and B_{II} as follows,

$$\boldsymbol{B_{joint}} = (I - S2_{11}S1_{22})^{-1}S2_{11}S1_{21}\boldsymbol{F_I} + (I - S2_{11}S1_{22})^{-1}S2_{12}\boldsymbol{B_{II}} \tag{3.48a}$$

$$\boldsymbol{F_{joint}} = (I - S1_{22}S2_{11})^{-1}S1_{21}\boldsymbol{F_I} + (I - S1_{22}S2_{11})^{-1}S1_{22}S2_{12}\boldsymbol{B_{II}} \tag{3.48b}$$

By inserting B_{joint} expression from (3.48a) into equation (3.46a) and inserting F_{joint} expression from (3.48b) into (3.47b) we get following equations

$$\boldsymbol{B_I} = [S1_{11} + S1_{12}(I - S2_{11}S1_{22})^{-1}S2_{11}S1_{21}]\boldsymbol{F_I} + [S1_{12}(I - S2_{11}S1_{22})^{-1}S2_{12}]\boldsymbol{B_{II}} \tag{3.49a}$$

$$\boldsymbol{F_{II}} = [S2_{21}(I - S1_{22}S2_{11})^{-1}S1_{21}]\boldsymbol{F_I} + [S2_{21}(I - S1_{22}S2_{11})^{-1}S1_{22}S2_{12} + S2_{22}]\boldsymbol{B_{II}} \tag{3.49b}$$

Expressions in (3.49a) and (3.49b) are in fact expanded version of the matrix in (3.45) hence submatrices of (3.45) can be concluded as follows,

$$S_{T11} = [S1_{11} + S1_{12}(I - S2_{11}S1_{22})^{-1}S2_{11}S1_{21}] \tag{3.50a}$$

$$S_{T12} = [S1_{12}(I - S2_{11}S1_{22})^{-1}S2_{12}] \tag{3.50a}$$

$$S_{T21} = [S2_{21}(I - S1_{22}S2_{11})^{-1}S1_{21}] \tag{3.50a}$$

$$S_{T22} = [S2_{21}(I - S1_{22}S2_{11})^{-1}S1_{22}S2_{12} + S2_{22}] \tag{3.50a}$$

3.6. Impedance Boundary Conditions for Corrugated Surfaces

Figure 3. 5. Structure of corrugated wall

Computational load of the model can be greatly reduced by changing corrugated walls of waveguide with impedance surfaces instead of applying MMT at all the grooves and plateaus through a structure. In order to obtain viable results surface impedance model should be a good approximation to said structure.

E and **H** fields can be related with fallowing equation when using impedance surface

$$\hat{n} \times \overline{\boldsymbol{E}} = \hat{n} \times \left[\overline{\overline{Z_s}}(\hat{n} \times \overline{\boldsymbol{H}})\right] \tag{3.51}$$

Where $\hat{n}$ is the unit normal vector to the surface and $\overline{\overline{Z_s}}$ is impedance dyadic.

$$\overline{\overline{Z_s}} = Z_x \hat{x}\hat{x} + Z_z \hat{z}\hat{z} \tag{3.52}$$

$\overline{\overline{Z_s}}$ in equations (3.51) and (3.52) models corrugated walls of a waveguide for periodic corrugations. Hence, transverse and longitudinal impedances are as given below (Uusitupa, 2006)

$$Z_x = \frac{\omega_g}{\omega_g + s} \frac{jk_g \eta_g}{\beta_1} \tan\left(\beta_1 h_g\right) \tag{3.53a}$$

$$Z_z = \frac{\omega_g}{\omega + s} j\eta_g \tan(k_g h_g) \tag{3.53b}$$

$$\beta_1 = \sqrt{k_g^2 - \left(\frac{\pi}{\omega_g}\right)^2} \tag{3.54}$$

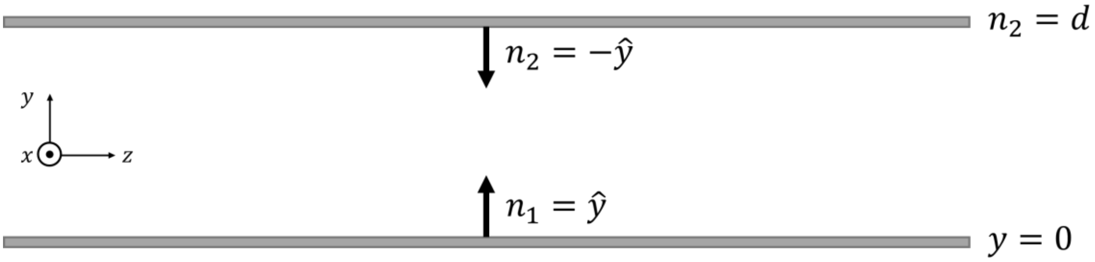

Figure 3. 6. Structure that represents waveguide when corrugated walls replaced with impedance surfaces.

Dispersion relations for TE ($E_z = E_y = H_x = 0$) modes for the structure in figure 3.6 can be obtained by applying impedance boundary at $y = 0$ and $y = d$. Equation 3.51 can be reduced to fallowing expressions for TE modes in structure given in Figure 3.6.

$$E_x = Z_x H_z \; for \; y = 0 \tag{3.55a}$$

$$E_x = -Z_x H_z \; for \; y = d \tag{3.55b}$$

Impedance boundary condition relations can be obtained at $y = 0$ by inserting expressions regarding E_x and E_z from equations 3.17 and 3.18 into equation 3.55a,

$$-\frac{j\omega\mu}{k_c}\left(-Asin(k_c 0) + Bcos(k_c 0)\right) = Z_x[Acos(k_c 0) + \sin\,(k_c 0)] \tag{3.56}$$

From equation above (3.56) an expression for A can be derived as follows

$$A = -\frac{j\omega\mu}{k_c Z_x} B \tag{3.57}$$

Impedance boundary condition relations can be obtained at $y = d$ by inserting expressions regarding E_x and E_z from equations 3.17 and 3.18 into equation 3.55b,

$$-\frac{j\omega\mu}{k_c}\left(-Asin(k_c d) + Bcos(k_C d)\right) = Z_x[Acos(k_c d) + \sin{(k_c d)}] \qquad (3.58)$$

After replacing A from equation 3.58 with its expression from equation 3.57 and performing some arrangements dispersion relation can be found as given below

$$\left[\frac{\omega^2\mu^2}{Z_x} + k_c^2\right]\sin(k_c d) - 2j\omega\mu k_c \cos{(k_c d)} = 0 \qquad (3.59)$$

Where Z_x is given in equation 3.53a.

In order to obtain scattering matrix, k_c values that makes dispersion relation zero can be found using numerical methods, after founding k_c values, corresponding propagation constants (β) can be found using equation 3.25 and scattering matrix can be constructed using equation 3.42.

Impedance expressions at equations 3.53a and 3.53b assume that dimensions of the grooves are much smaller than the wavelength of the travelling wave and distance between grooves are close to zero if these conditions don’t met result will not match to experimental values.

4. RESULTS AND DISCUSSION

4.1. Verifications of The Model

From equations (3.34) and (3.37) it's obvious that in order to find exact values of S parameters, infinitely many numbers of modes need to be considered in each region. But in order to calculate S parameters using computers we need to truncate modes at some point. In this Chapter accuracy of mathematical formulation and effects of mode truncation on accuracy is investigated on various geometries. Results are compared with CST Studio simulations; simulations are done with a computer that has six core intel $i5\ 10400$ processor. The dimensions of each waveguide region are sampled from Gaussian distributed random numbers. Mean value of random numbers for width and length of waveguide regions is $250mm$ and $500mm$ respectively, standard deviation of these random numbers is $100mm$ and $250mm$ respectively.

4.1.1. Waveguide with four discontinuities

Figure 4. 1. Waveguide with four discontinuities

The structure above (Figure 4.1) was constructed with randomly chosen dimensions. Cutoff frequency of the narrowest region is $1.050\ GHz$.

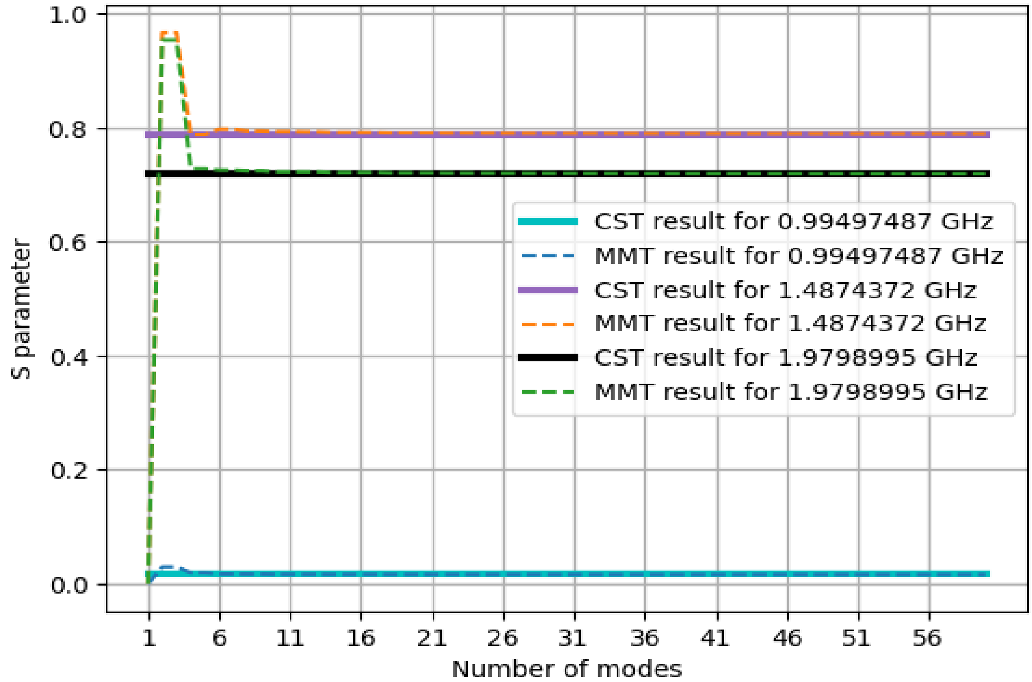

Figure 4. 2. Graph that shows convergence behavior for the waveguide (Figure 4.5)

As seen from the graphs in Figure 4.2 and Figure 4.3 mode matching technique starts to converge to CST simulation results rapidly, after three modes error becomes less than 0.01.

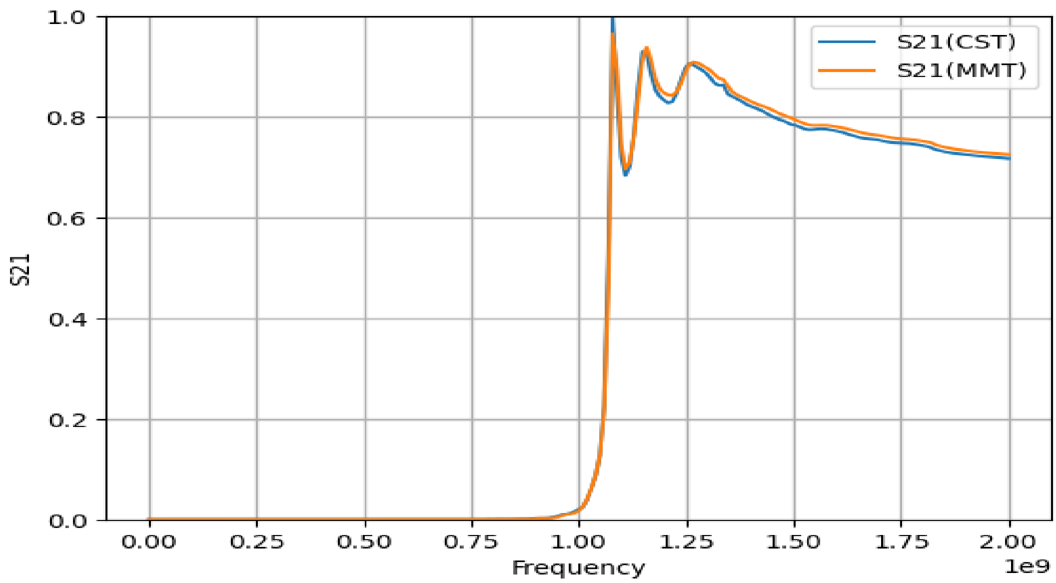

Figure 4. 3 S21 comparison between CST and MMT for given waveguide.

Figure 4.4. shows that implemented mode matching technique is highly adequate for given waveguide with four discontinuities.

4.1.2. Waveguide with six discontinuities

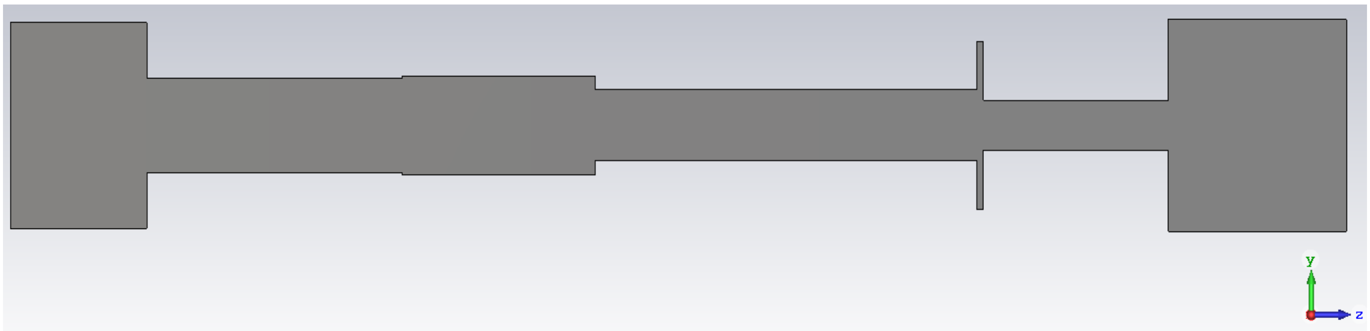

Figure 4. 4. Geometry of waveguide with six discontinuities

Structure given above (Figure 4.5) has cutoff frequency of $f_{cutoff} = 1.49\ GHz$ at its narrowest region.

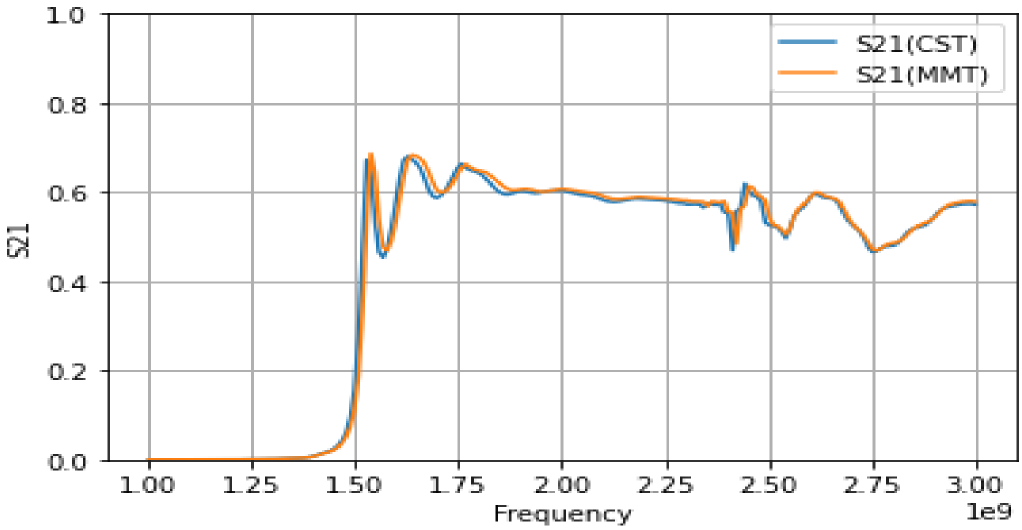

Figure 4. 5. S21 comparison between MMT and CST for the waveguide (Figure 4.4)

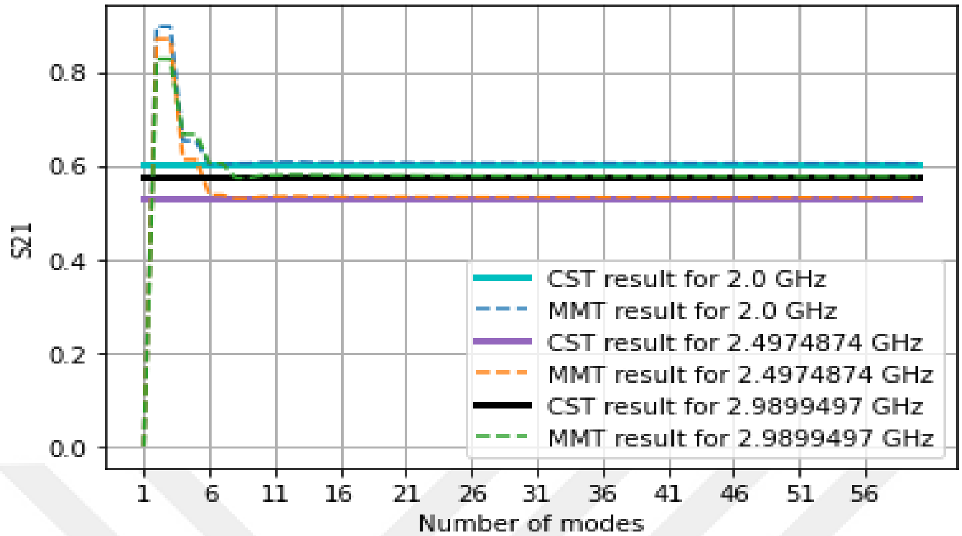

Figure 4. 6. Graph that shows convergence behavior of MMT for the waveguide (Figure 4.4)

As can be seen from graphs (Figure 4.5 and Figure 4.6) waveguide in Figure 4.5 becomes pretty close to CST simulation results, after 7 modes error becomes less than percent as opposed to 3 modes for waveguide in Figure 4.1.

4.1.3. Waveguide with eight discontinuities

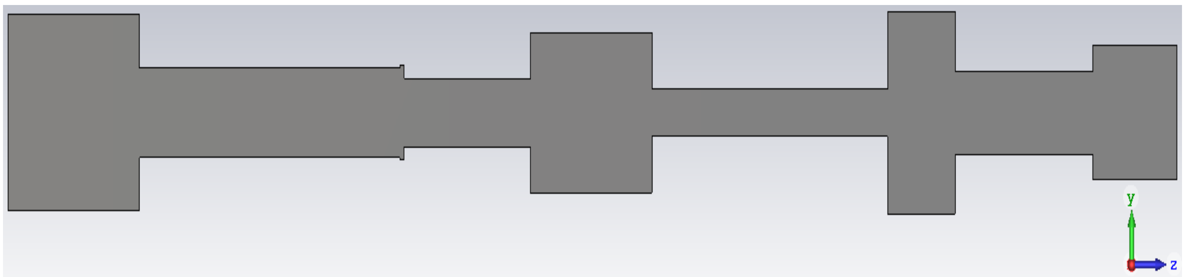

Figure 4. 7. Geometry of waveguide with eight discontinuities

Structure given above (Figure 4.7) also has cutoff frequency of $f_{cutoff} = 1.49\ GHz$, like previous waveguide (Figure 4.4), at its narrowest region.

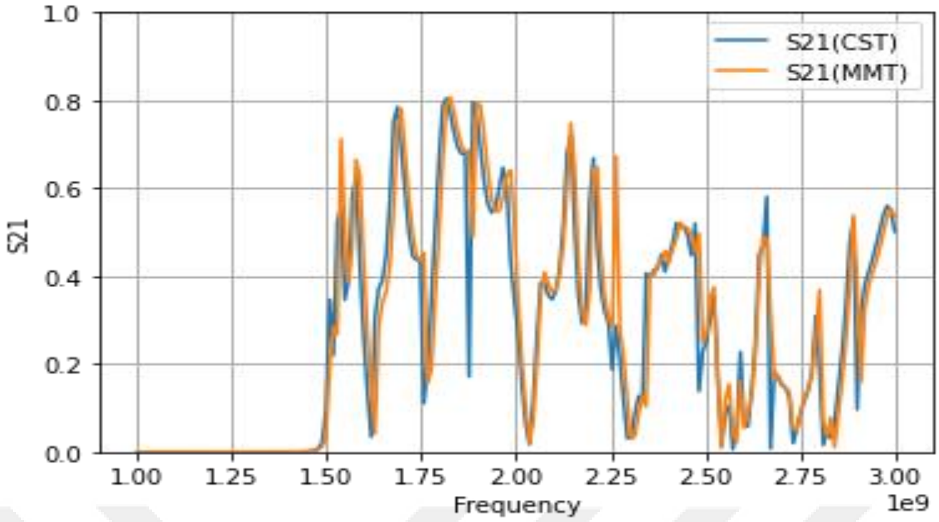

Figure 4. 8. S21 comparison between MMT and CST for the waveguide (Figure 4.7)

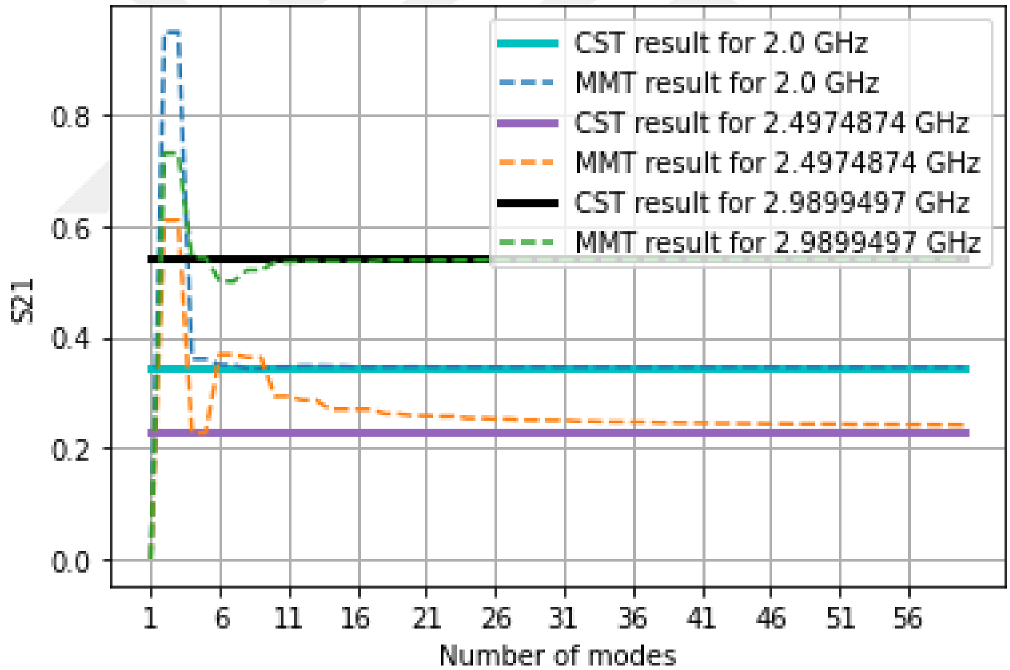

Figure 4. 9. Graph that shows convergence behavior of MMT for the waveguide (Figure 4.7)

For the given geometry (Figure 4.7) MMT results begin to converge around 15 modes, but at 15 mode it's a little distant to CST simulation result but after 31 modes error between CST and MMT becomes less than two percent.

4.1.4. Waveguide with ten discontinuities

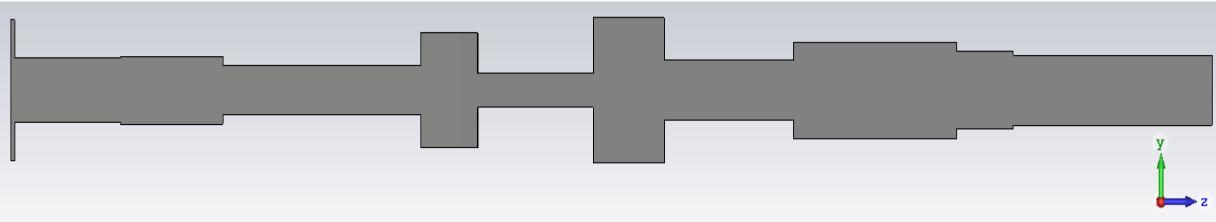

Figure 4. 10. Geometry of waveguide with ten discontinuities

This waveguide (Figure 4.10) has the same cutoff frequency at the narrowest region with previous one which is 1.49GHz.

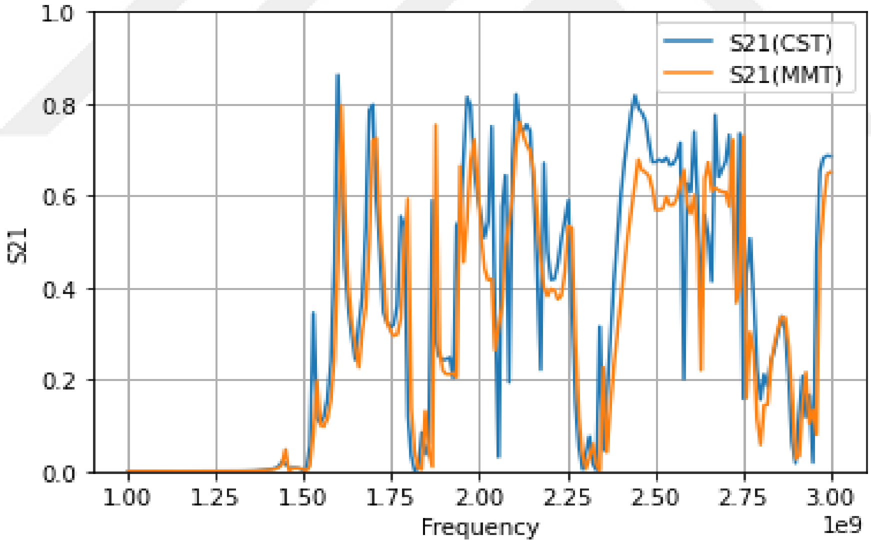

Figure 4. 11. S21 comparison between MMT and CST for the waveguide (Figure 4.10)

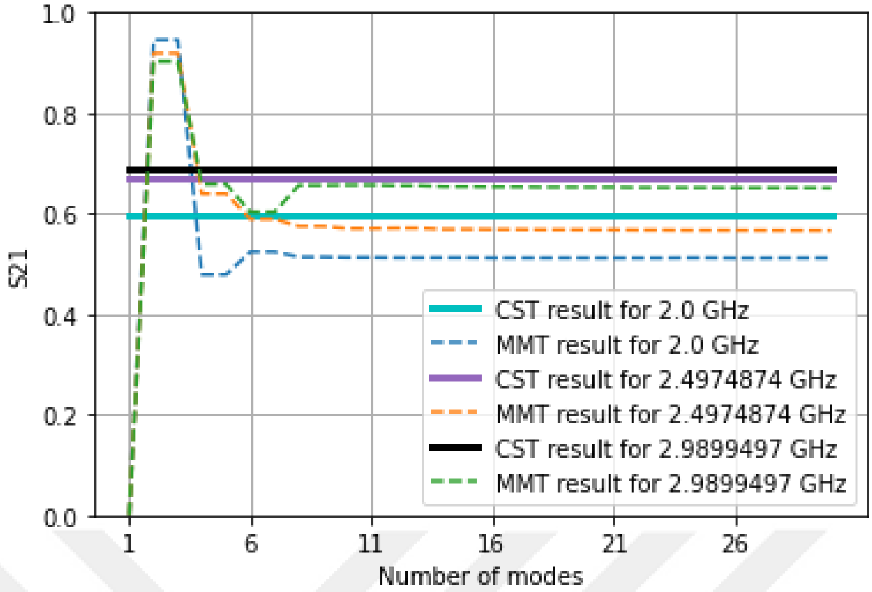

Figure 4. 12. Graph that shows convergence behavior of MMT for the waveguide (Figure 4.7)

As can be seen from Figure 4.12 MMT results start to converge after 10 modes albeit it's a bit off from CST simulation results. Even though MMT results (Figure4.11, Figure 4.8, Figure 4.5, Figure 4.3) are sufficiently similar to CST simulation results and converge to a value around 15 modes, noticeable differences start to appear when structure becomes more intricate. The blame for this discrepancy when structure becomes more complex is not entirely on proposed model because CST needs more meshes for complex structures, but there is a limit for how high we can set those meshes because it's expected from simulations to finish at reasonable time, so this inadequacy in mesh amount also adds to the discrepancy. Hence mode matching technique calculations takes fraction of the time needed by the simulations, these high simulation runtimes for long cascaded structures are one of the main incentives of this study. After these steps, one can be confident that developed MMT implementation for cascaded structure gives accurate results so from now on CST simulations will not be considered because it is not needed also it takes too much time when there is high mesh detail and if more conservative values are chosen for mesh details MMT results will be more accurate.

4.2. Corrugated Structures

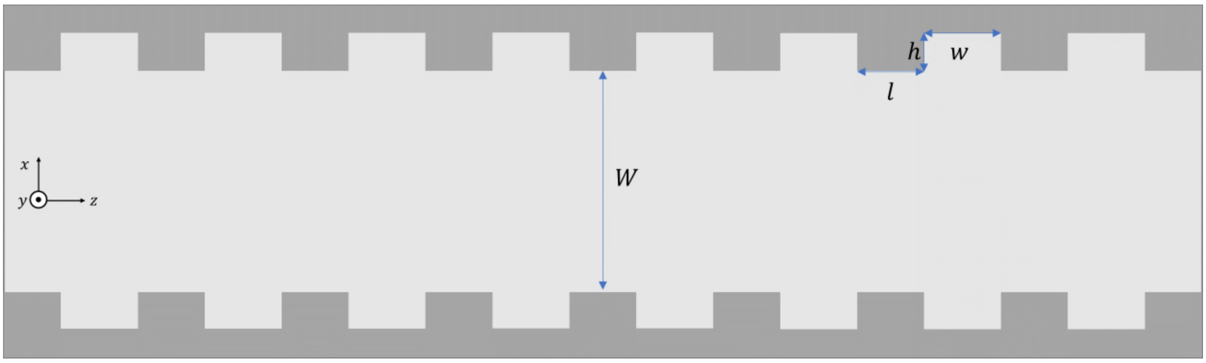

Figure 4. 13. Structure of parallel plate waveguide with corrugated walls

Above in Figure 4.13 structure of parallel plate waveguide with corrugated walls is given. In this chapter waveguides with corrugated walls that have various number of grooves will be examined.

Dimensions for each groove ($w = 7$mm and $h = 51$mm) and waveguide width ($W = 250$) will stay same through the waveguide but periodicity of each corrugation will be different and length of each interval between two groove is sampled from normally distributed random numbers ($l = normal(\mu, \sigma)$). Results from waveguides with nonperiodic corrugations will be compared with periodic ones that have intervals between grooves equal to mean values of nonperiodic one.

4.2.1. Corrugations with 40 grooves

In this chapter MMT implementation had been run for waveguide with nonperiodic corrugations, the distance between grooves is sampled from normally distributed random numbers with $\mu = 100\text{mm}\ \ and\ \sigma = 25\text{mm}$ and difference between nonperiodic and periodic corrugations are inspected, the distance between grooves for periodic corrugations are a fixed value, equal to mean of nonperiodic one, in this case $100mm$.

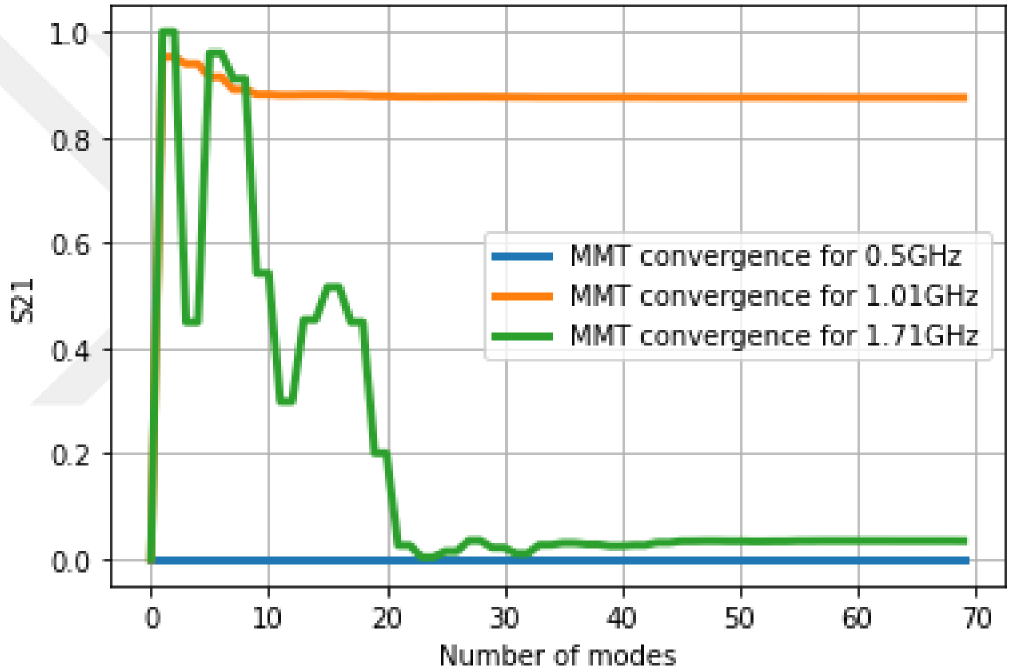

Figure 4. 14. Graph that shows convergence behavior of waveguide with nonperiodic corrugations that has $\sigma_l = 25\text{mm}$.

Figure 4.14 shows that S21 parameters start to converge around 30 modes.

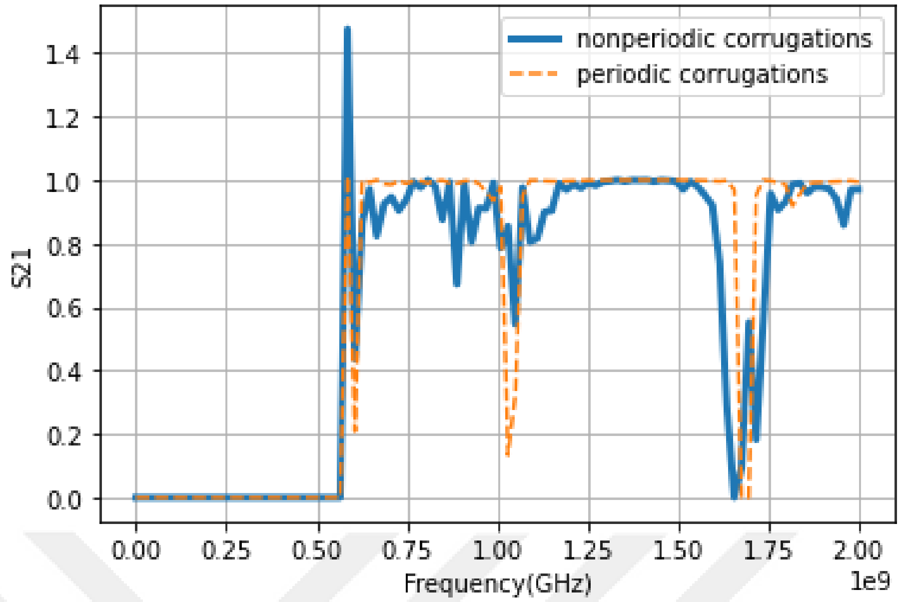

Figure 4. 15. Comparison of S21 between waveguides with nonperiodic and periodic corrugations with standard deviation $\sigma_l = 25$mm.

As can be seen from Figure 4.14 waveguides with nonperiodic and periodic corrugations for $\sigma_l = 25mm$ looks roughly similar but nonperiodic one has some irregularities introduced by nonperiodic shape also nonperiodic one has wider bands at rejected frequencies around 1.65 GHz and does not reject frequencies around 1 GHz as much as the periodic one so by taking advantage of these king behaviors of nonperiodic corrugations filters with desired characteristics may be constructed.

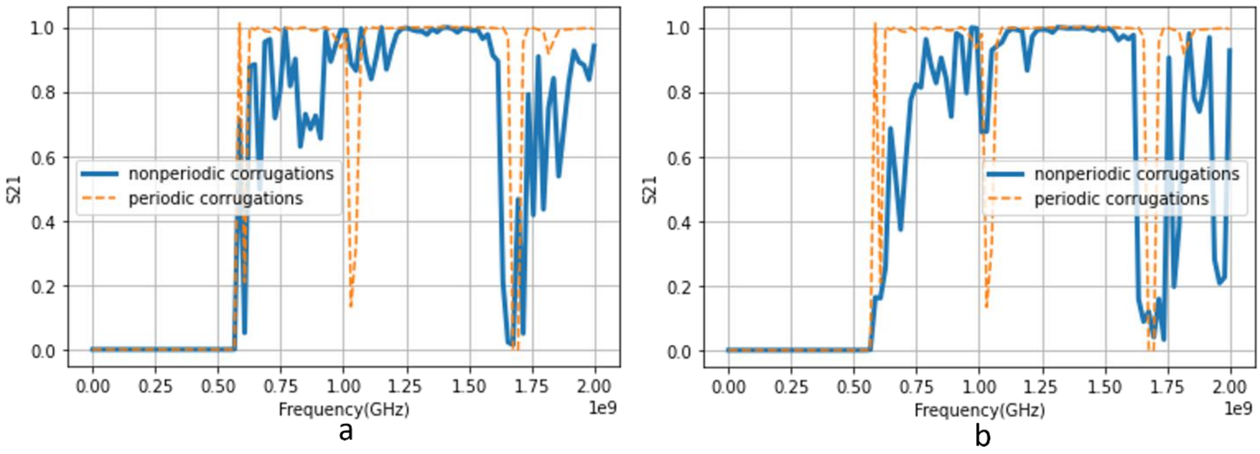

Figure 4. 16. Comparison of S21 between waveguides with nonperiodic and periodic corrugations (a- $\sigma_l = 50$mm b- $\sigma_l = 75$mm)

From graphs above (Figure 4.16) it can be concluded when standard deviation of the interval between grooves increased further, even though it still resembles the periodic one it deteriorates further.

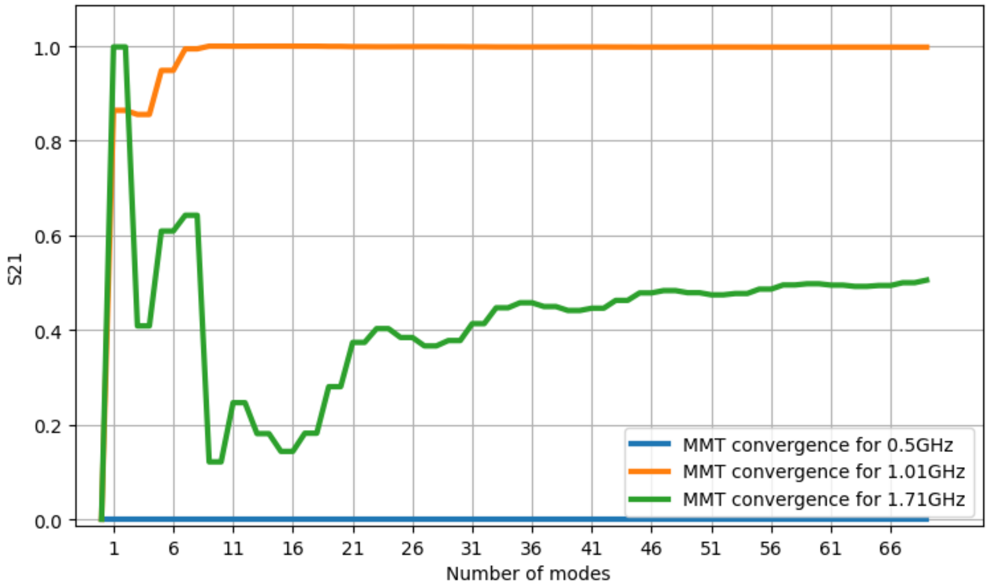

Figure 4. 17. Graph that shows convergence behavior of waveguide with nonperiodic corrugations that has $\sigma_l = 75$mm.

Figure 4.17 shows that increasing the standard deviation of distance between each groove not just affects the S parameters, it also affects how many modes it takes to settle to a stable value as in graph shows it took 45 modes to settle in this case.

4.2.2. Corrugations with 60 grooves

Structure is constructed as in the same manner in previous section, with 60 grooves and distance between each groove assigned randomly using normal distribution using mean and standard deviation as $\mu = 100$mm and $\sigma = 50$mm and then using $\mu = 100$mm and $\sigma = 75$mm

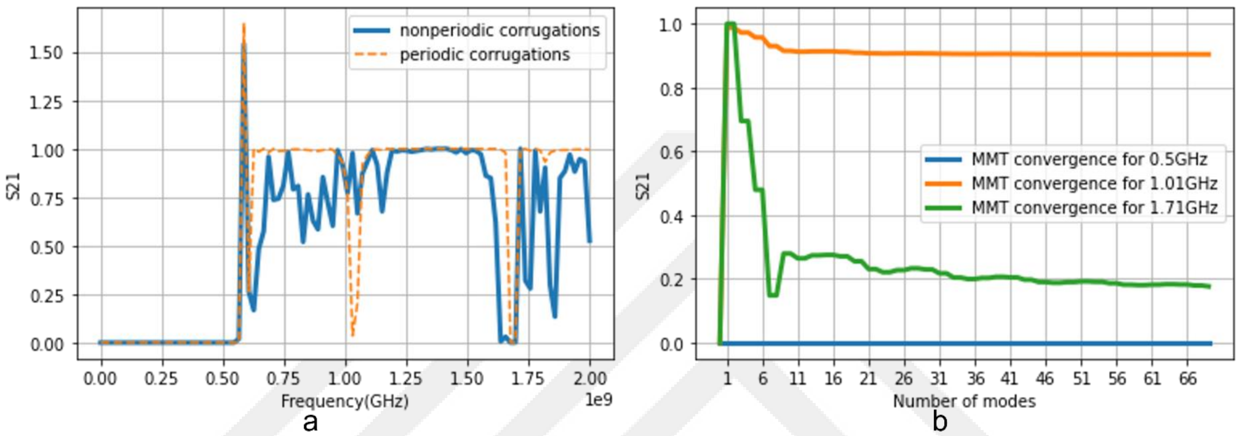

Figure 4. 18. for $\sigma_l = 50$mm a- S21 parameter b- Convergence behavior

It can be concluded from above graph (Figure 4.18) for same standard deviation values waveguide that has more corrugations is a bit more distant to its periodic counterpart.

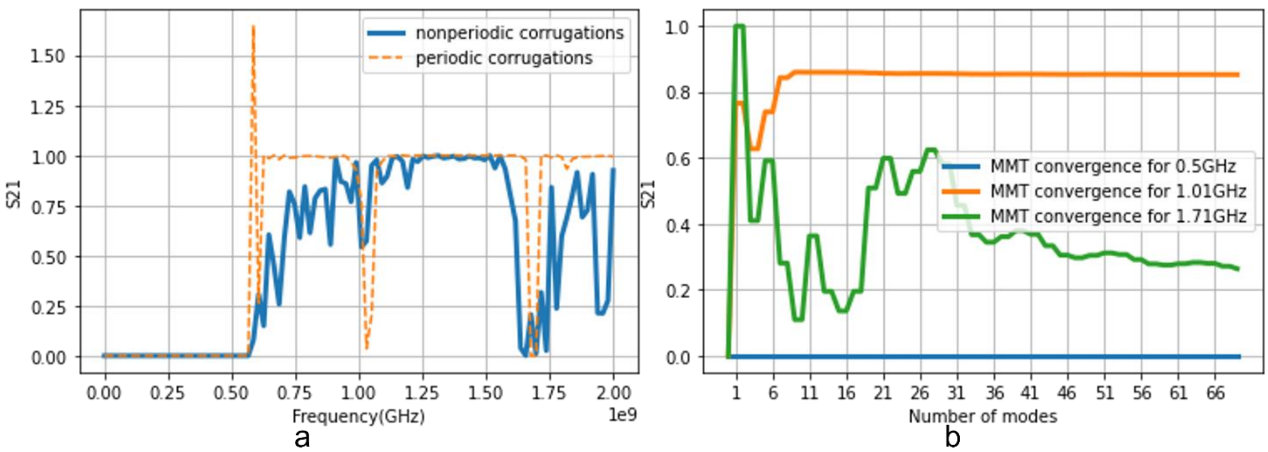

Figure 4. 19. for $\sigma_l = 75$mm a- S21 parameter b- Convergence behavior

Figure 4.19 shows that when we increase standard deviation S21 parameters becomes more distant to its periodic counterpart, and it takes more modes to settle to a stable value for this case it starts to settle around 65 modes.

4.2.3. Replacing Corrugations with Impedance Surfaces

In order to reduce computational complexity, corrugated wall can be replaced with impedance surfaces, but impedance surface can have its own drawbacks such as not giving accurate results when structure is deviated a little more than model can handle for example in our structure if grooves get a little bigger compared to wavelength results will start to differentiate from its real values.

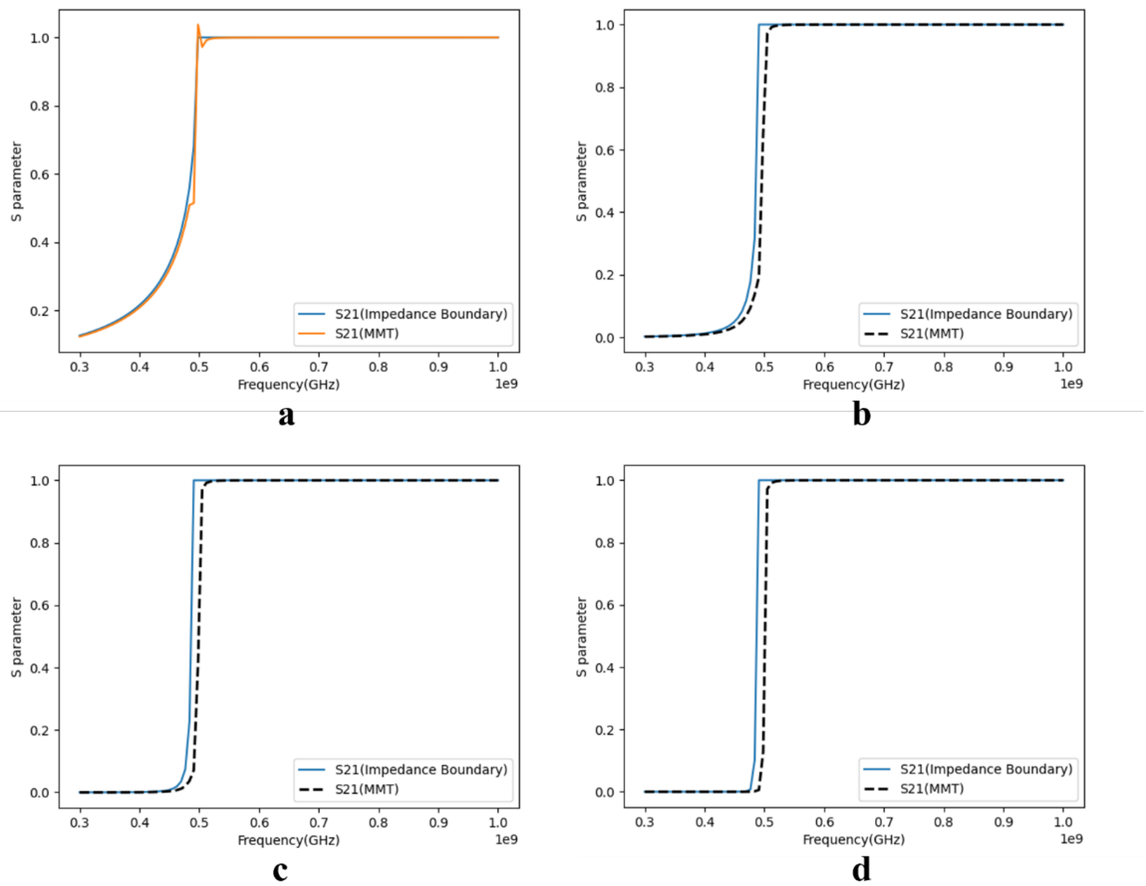

Figure 4. 20. Impedance Boundary vs MMT comparison for a corrugated waveguide with; w_g=5.01mm(a), 15.01mm(b), 25.01mm(c), 50.01mm(d); s=0.001mm;H_g =5.01mm; W (waveguide width)=301mm

Figure 4.20 shows MMT vs Impedance Surface comparisons of waveguides with different groove widths, when groove widths are much smaller than the wavelength MMT and Impedance surface results are pretty much the same but when widths begin to increase results gets a bit off each other because it starts to get comparable values to wavelength.

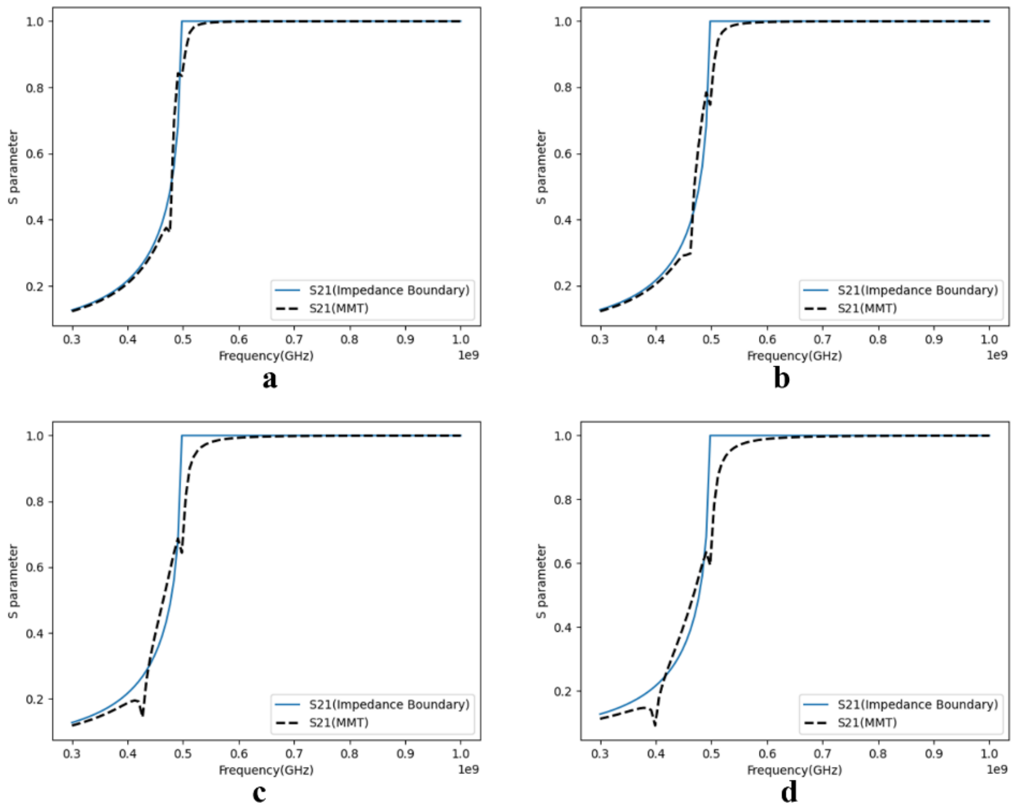

Figure 4. 21. Impedance Boundary vs MMT comparison for a corrugated waveguide with; w_g=5.01mm; s=0.001mm; H_g=15.01mm(a), 25.01mm(b), 50.01mm(c), 75.01mm(d); W=301mm(waveguide width)

Figure 4.21 shows Impedance Surface vs MMT comparisons for different values of groove heights and it shows similar behavior to Figure 4.20 such as when groove heights get bigger comparably to wavelength discrepancies of results increase.

5. CONCLUSIONS AND RECOMMENDATIONS

In this study a formulation for cascaded discontinuities for parallel plate waveguides developed. Implementation of analytical methods are verified via comparing results with CST Studio simulations.

Implementation developed in this study can be used not for only analysis of parallel plate waveguide with corrugations, it can be used for parallel plate waveguides that contains arbitrary number of discontinuities.

Results obtained in this study show that characteristics of waveguide with nonperiodic corrugations are very similar for low standard deviation of distances between grooves. When standard deviation or number of grooves increases results become more distant to periodic one.

Even for increased values of standard deviation results are surprisingly resembles periodic one with some characteristic changes such as wider band of frequency rejection in already rejected frequencies at waveguide with periodic corrugations sometimes nonperiodic one will allow frequencies that blocked by its periodic counterparts. One can take advantage of these emerging characteristics to obtain certain characteristics. For example, in this study periodicity of each groove is assigned randomly, but via assigning distance between each grooves deliberately in such a way that it will give us desired characteristics also when assigning those values some clever optimization algorithms and machine learning methods can be utilized.

When using impedance boundary conditions for the corrugated walls, it gives accurate results if groove dimensions are much smaller than wavelength and it also requires the distance between two corrugations to be close to zero in order to work. So, impedance boundary conditions are not as viable as MMT for aperiodic randomized structures, it may have less computational requirements but it also prone to deviate from real values when dimensions of the structure get out of its operation range.

REFERENCES

R Coccioli, G Pelosi, R Ravanelli, “A mode matching-integral equation technique for the analysis and design of corrugated horns” *Aerospace Science and Technology*, Volume 2, Issue 2, 1998, Pages 121-128, ISSN 1270-9638, https://doi.org/10.1016/S0034-1223(98)80010-9.

F. Ghasemifard, M. Ebrahimpouri, M. Norgren and O. Quevedo-Teruel, "Mode matching analysis of two dimensional glide-symmetric corrugated metasurfaces," *2017 11th European Conference on Antennas and Propagation (EUCAP)*, 2017, pp. 749-751, doi: 10.23919/EuCAP.2017.7928533.

I.Hanninen and K. Nikoskinen, "Implementation of Method of Moments for Numerical Analysis of Corrugated Surfaces With Impedance Boundary Condition," in *IEEE Transactions on Antennas and Propagation*, vol. 56, no. 1, pp. 278-281, Jan. 2008, doi: 10.1109/TAP.2007.913171.

Z. Sipus and P. Kildal, "Green's functions for corrugated surface derived by asymptotic corrugation boundary conditions," *IEEE Antennas and Propagation Society International Symposium. 1996 Digest*, 1996, pp. 322-325 vol.1, doi: 10.1109/APS.1996.549604.

A. Wexler, "Solution of Waveguide Discontinuities by Modal Analysis," in *IEEE Transactions on Microwave Theory and Techniques*, vol. 15, no. 9, pp. 508-517, September 1967, doi: 10.1109/TMTT.1967.1126521.

T. M. Uusitupa, "Usability Studies on Approximate Corrugation Models in Scattering Analysis," in *IEEE Transactions on Antennas and Propagation*, vol. 54, no. 9, pp. 2486-2496, Sept. 2006, doi: 10.1109/TAP.2006.880774.